Using the Euler–Lagrange variational principle to obtain flow relations for generalized Newtonian fluids

Taha Sochi

Using Euler-Lagrange Variational Principle to Obtain Flow Relations for Generalized Newtonian Fluids

Taha Sochi*

October 29, 2018

*University College London - Department of Physics & Astronomy - Gower Street - London - WC1E 6BT. Email: t.sochi@ucl.ac.uk.

Contents

List of Figures

Abstract

Euler-Lagrange variational principle is used to obtain analytical and numerical flow relations in cylindrical tubes. The method is based on minimizing the total stress in the flow duct using the fluid constitutive relation between stress and rate of strain. Newtonian and non-Newtonian fluid models; which include power law, Bingham, Herschel-Bulkley, Carreau and Cross; are used for demonstration.

Keywords: Euler-Lagrange variational principle; fluid mechanics; generalized Newtonian fluid; capillary flow; pressure-flow rate relation; Newtonian; power law; Bingham; Herschel-Bulkley; Carreau; Cross.

1 Introduction

Several methods are in use to derive relations between pressure, p, and volumetric flow rate, Q, in tubes and conduits. These methods include the application of first principles of fluid mechanics with utilizing the fluid basic properties [1–3], the use of Navier-Stokes equations [4], the lubrication approximation [5], and Weissenberg-Rabinowitsch-Mooney relation [1–3, 6]. Numerical methods related to these analytical formulations, such as finite element and similar meshing techniques [7], are also in use when analytical expressions are not available.

However, we are not aware of the use of the Euler-Lagrange variational principle to derive p-Q relations in general and in capillaries in particular despite the fact that this principle is more intuitive and natural to use as it is based on a more fundamental physical principle which is minimizing the total stress combined with the utilization of the fluid constitutive relation between stress and rate of strain.

The objective of this paper is to outline this method demonstrating its application to Newtonian and some time-independent non-Newtonian fluids and featuring its applicability numerically as well as analytically. In the following, we assume a laminar, axi-symmetric, incompressible, steady, viscous, isothermal, fully-developed flow for generalized Newtonian fluids moving in cylindrical tubes where no-slip at wall condition [8] applies and where the flow velocity profile has a stationary derivative point at the middle of the tube ($r = 0$) meaning the profile has a blunt rounded vertex.

2 Method

The constitutive relation for generalized Newtonian fluids in shear flow is given by

$$\tau = \mu\gamma \tag{1}$$

where τ is the shear stress, γ is the rate of shear strain, and μ is the shear viscosity which generally is a function of the rate of shear strain. It is physically intuitive that the flow velocity profile in a tube (or in a flow path in general) will adjust itself to minimize the total stress which is given by

$$\tau_t = \int_{\tau_c}^{\tau_w} d\tau = \int_0^R \frac{d\tau}{dr} dr = \int_0^R \frac{d}{dr}(\mu\gamma)\, dr = \int_0^R \left(\gamma \frac{d\mu}{dr} + \mu \frac{d\gamma}{dr}\right) dr \tag{2}$$

where τ_t is the total stress, τ_c and τ_w are the shear stress at the tube center and tube wall respectively, and R is the tube radius. The total stress, as given by Equation 2, can be minimized by applying the Euler-Lagrange variational principle which, in its most famous form, is given by

$$\frac{\partial f}{\partial y} - \frac{d}{dx}\left(\frac{\partial f}{\partial y'}\right) = 0 \tag{3}$$

where

$$x \equiv r, \quad y \equiv \gamma, \quad f \equiv \gamma \frac{d\mu}{dr} + \mu \frac{d\gamma}{dr}, \quad \text{and} \quad \frac{\partial f}{\partial y'} \equiv \frac{\partial}{\partial \gamma'}\left(\gamma \frac{d\mu}{dr} + \mu \frac{d\gamma}{dr}\right) = \mu \tag{4}$$

However, to simplify the derivation we use here another form of the Euler-Lagrange principle which is given by

$$\frac{d}{dx}\left(f - y' \frac{\partial f}{\partial y'}\right) - \frac{\partial f}{\partial x} = 0 \tag{5}$$

that is

$$\frac{d}{dr}\left(\gamma \frac{d\mu}{dr} + \mu \frac{d\gamma}{dr} - \mu \frac{d\gamma}{dr}\right) - \frac{\partial}{\partial r}\left(\gamma \frac{d\mu}{dr} + \mu \frac{d\gamma}{dr}\right) = 0 \tag{6}$$

i.e.

$$\frac{d}{dr}\left(\gamma\frac{d\mu}{dr}\right) - \frac{\partial}{\partial r}\left(\gamma\frac{d\mu}{dr} + \mu\frac{d\gamma}{dr}\right) = 0 \tag{7}$$

Since ordinary derivative is a special case of partial derivative, we can write this equation as

$$\frac{\partial}{\partial r}\left(\gamma\frac{d\mu}{dr} - \gamma\frac{d\mu}{dr} - \mu\frac{d\gamma}{dr}\right) = 0 \tag{8}$$

that is

$$\frac{\partial}{\partial r}\left(\mu\frac{d\gamma}{dr}\right) = 0 \tag{9}$$

In the following sections the use of this equation will be demonstrated to derive p-Q flow relations for generalized Newtonian fluids.

2.1 Newtonian

For Newtonian fluids, the viscosity is constant that is

$$\mu = \mu_o \tag{10}$$

and hence Equation 9 becomes

$$\frac{\partial}{\partial r}\left(\mu_o\frac{d\gamma}{dr}\right) = 0 \tag{11}$$

On integrating once with respect to r we obtain

$$\mu_o\frac{d\gamma}{dr} = A \tag{12}$$

where A is a constant. Hence

$$\gamma = \frac{1}{\mu_o}(Ar + B) \tag{13}$$

where B is another constant. Now from the two boundary conditions at $r = 0$ and $r = R$, A and B can be determined, that is

$$\gamma(r = 0) = 0 \qquad \Rightarrow \qquad B = 0 \tag{14}$$

and

$$\gamma(r = R) = \frac{\tau_w}{\mu_o} = \frac{PR}{2L\mu_o} = \frac{AR}{\mu_o} \qquad \Rightarrow \qquad A = \frac{P}{2L} \tag{15}$$

where τ_w is the shear stress at the tube wall, P is the pressure drop across the tube and L is the tube length. Hence

$$\gamma(r) = \frac{P}{2L\mu_o} r \tag{16}$$

On integrating this with respect to r the standard Hagen-Poiseuille parabolic velocity profile is obtained, that is

$$v(r) = \int dv = \int \frac{dv}{dr} dr = \int \gamma dr = \int \frac{P}{2L\mu_o} r dr = \frac{P}{4L\mu_o} r^2 + D \tag{17}$$

where $v(r)$ is the fluid axial velocity at r and D is another constant which can be determined from the no-slip at wall boundary condition, that is

$$v(r = R) = 0 \qquad \Rightarrow D = -\frac{PR^2}{4L\mu_o} \tag{18}$$

that is

$$v(r) = \frac{-P}{4L\mu_o}\left(R^2 - r^2\right) \tag{19}$$

where the minus sign at the front arises from the fact that the pressure gradient is opposite in direction to the flow velocity vector. The volumetric flow rate will then follow by integrating the flow velocity profile with respect to the cross sectional area, that is

$$Q = \int_0^R |v| \, 2\pi r dr = \frac{\pi P}{2L\mu_o} \int_0^R \left(R^2 - r^2\right) r dr = \frac{\pi P R^4}{8L\mu_o} \tag{20}$$

which is the well-known Hagen-Poiseuille flow relation.

2.2 Power Law

For power law fluids, the viscosity is given by

$$\mu = k\gamma^{n-1} \tag{21}$$

On applying Euler-Lagrange variational principle (Equation 9) we obtain

$$\frac{\partial}{\partial r}\left(k\gamma^{n-1}\frac{d\gamma}{dr}\right) = 0 \tag{22}$$

On integrating once with respect to r we obtain

$$k\gamma^{n-1}\frac{d\gamma}{dr} = A \tag{23}$$

On separating the two variables and integrating both sides we obtain

$$\gamma = \sqrt[n]{\frac{n}{k}\left(Ar + B\right)} \tag{24}$$

where A and B are constants which can be determined from the two boundary conditions, that is

$$\gamma\left(r = 0\right) = 0 \qquad \Rightarrow \qquad B = 0 \tag{25}$$

and

$$\gamma\left(r=R\right)=\sqrt[n]{\frac{\tau_w}{k}}=\sqrt[n]{\frac{PR}{2Lk}}=\sqrt[n]{\frac{n}{k}AR}\qquad\Rightarrow\qquad A=\frac{P}{2nL}\tag{26}$$

and therefore

$$\gamma=\sqrt[n]{\frac{P}{2kL}}r^{1/n}\tag{27}$$

On integrating this with respect to r the power law velocity profile is obtained, that is

$$v\left(r\right)=\int dv=\int\frac{dv}{dr}dr=\int\gamma dr=\int\sqrt[n]{\frac{P}{2kL}}r^{1/n}dr=\frac{n}{n+1}\sqrt[n]{\frac{P}{2kL}}r^{1+1/n}+D\tag{28}$$

where D is another constant. From the no-slip at wall boundary condition

$$v\left(r=R\right)=0\qquad\Rightarrow D=-\frac{n}{n+1}\sqrt[n]{\frac{P}{2kL}}R^{1+1/n}\tag{29}$$

that is

$$v\left(r\right)=\frac{-n}{n+1}\sqrt[n]{\frac{P}{2kL}}\left(R^{1+1/n}-r^{1+1/n}\right)\tag{30}$$

The volumetric flow rate will then follow by integrating the velocity profile with respect to the cross sectional area, that is

$$Q=\int_0^R\left|v\right|2\pi rdr=\frac{2\pi n}{n+1}\sqrt[n]{\frac{P}{2kL}}\int_0^R\left(R^{1+1/n}-r^{1+1/n}\right)rdr$$

$$=\frac{\pi n}{3n+1}\sqrt[n]{\frac{P}{2kL}}R^{3+1/n}\tag{31}$$

which is mathematically equivalent to the expressions derived in [1–3, 5] using other

methods.

3 Numerical Implementation

For generalized Newtonian fluids with complex constitutive relations, it may be very difficult, or even impossible, to obtain a flow analytical solution from the Euler-Lagrange principle. In this case, the variational method can be used as a basis for a numerical method by employing Equation 9 to obtain the rate of shear strain as an explicit or implicit function of r which is then numerically solved and integrated to obtain the flow velocity profile which, in its turn, is numerically integrated to obtain the p-Q relation. For the fluids which have an explicit relation between the rate of strain and radius, such as Newtonian and power law fluids (refer to Equations 16 and 27), the rate of strain can be computed directly for each r. However, for the fluids which have no such explicit relation, such as Bingham, Herschel-Bulkley, Carreau and Cross (refer to Equations 33, 36, 39 and 46), a numerical solver, based for instance on a bisection method, is required to find the rate of strain as a function of radius. A numerical integration scheme; such as midpoint, trapezium or Simpson rule; can then be utilized to integrate the strain rate with respect to radius to obtain the velocity profile in the first stage, and to integrate the velocity profile with respect to the cross sectional area to get the volumetric flow rate in the second stage.

The constant of the first integration (strain rate with respect to radius) is incorporated within a boundary condition by starting at the wall with zero velocity ($v = 0$); the velocity growth at the next inner ring of the tube cross section, obtained from numerically integrating the shear rate over radius, is then added incrementally to the velocity of the neighboring previous outer ring to obtain the velocity at the inner ring. The volumetric flow rate is then computed by multiplying the velocity of the ring with its cross sectional area and adding these partial

flow rate contributions to obtain the total flow rate. This method is applied, for the purpose of test and validation, to the Newtonian and power law fluids, for which analytical solutions are available, and the numerical results were compared to these analytical solutions. A sample of these comparisons are provided in Figures 1 and 2. As seen, the numerical solutions converge fairly quickly to the analytical solutions; hence confirming the reliability of this numerical method and its theoretical foundations. It should be remarked that the numerical results presented in the following sections were obtained by using three numerical integration schemes: midpoint, trapezium and Simpson rules. In all cases the three schemes converged to the same value although with different convergence rate. For the fluids with an implicit γ-r relation, a bisection numerical solver was used to obtain γ as a function of r.

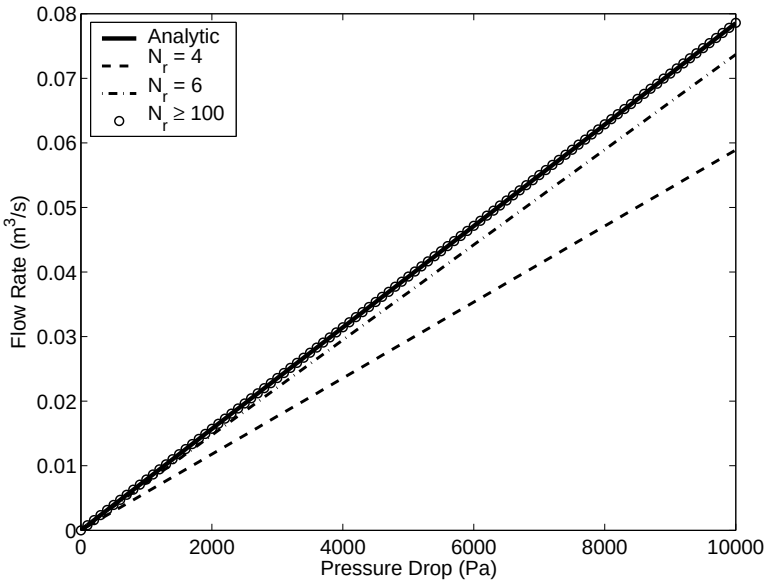

Figure 1: Q versus P plot for numeric solutions of a typical Newtonian fluid with $\mu_o = 0.005$ Pa.s, flowing in a tube with $L = 0.1$ m and $R = 0.01$ m for r-discretization $N_r = 4$, $N_r = 6$ and $N_r \geq 100$ alongside the analytical solution (Equation 20).

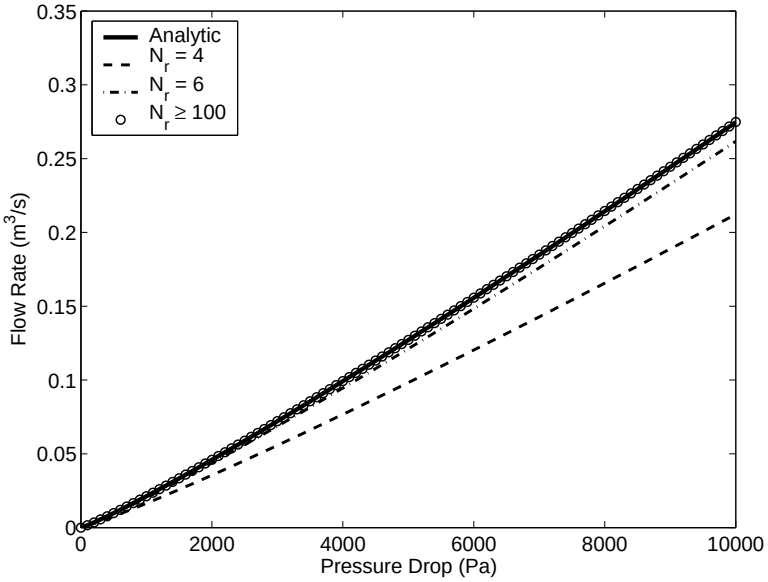

Figure 2: Q versus P plot for numeric solutions of a typical power law fluid with $n = 0.9$ and $k = 0.005$ Pa.s^n, flowing in a tube with $L = 0.1$ m and $R = 0.01$ m for r-discretization $N_r = 4$, $N_r = 6$ and $N_r \geq 100$ alongside the analytical solution (Equation 31).

4 Yield Stress Fluids

Experimenting with the use of Euler-Lagrange principle on different fluids, we tested this method on some yield stress fluids, specifically Bingham plastic and Herschel-Bulkley models, despite our awareness of the limitation of this method and its restriction to fluids which makes it inapplicable to yield stress materials since the solid-like plug flow at the center of the tube invalidates this assumption.

For Bingham fluids, the viscosity is given by [1, 2, 9, 10]

$$\mu = \frac{\tau_o}{\gamma} + C \tag{32}$$

where τ_o is the yield stress and C is the fluid consistency factor. On applying Euler-Lagrange variational principle (Equation 9) and following the method outlined in the Newtonian and power law fluid sections we obtain

$$\tau_o \ln \gamma + C\gamma = Ar + B \tag{33}$$

where A and B are the constants of integration. As seen in the last equation, the boundary condition at $r = 0$ cannot be used to find B because $\gamma = 0$ is a singularity point. We therefore followed the non-yield stress fluid style and arbitrarily set $B = 0$. On applying the other boundary condition at $r = R$, we obtain

$$A = \frac{\tau_o}{R} \ln \left(\frac{PR}{2LC} - \frac{\tau_o}{C} \right) + \left(\frac{P}{2L} - \frac{\tau_o}{R} \right) \tag{34}$$

For Herschel-Bulkley fluids, the viscosity is given by [1, 2, 9, 10]

$$\mu = \frac{\tau_o}{\gamma} + C\gamma^{n-1} \tag{35}$$

Following a similar approach to that outlined in the Bingham part, the following relation was obtained

$$\tau_o \ln \gamma + \frac{C}{n}\gamma^n = Ar \tag{36}$$

where

$$A = \frac{\tau_o}{R} \ln \left(\left(\frac{PR}{2LC} - \frac{\tau_o}{C} \right)^{1/n} \right) + \frac{1}{n} \left(\frac{P}{2L} - \frac{\tau_o}{R} \right) \tag{37}$$

These γ-r relations (i.e. Equation 33 for Bingham and Equation 36 for Herschel-Bulkley) were then solved for γ at each r and numerically integrated to obtain the flow velocity profile first and volumetric flow rate second. The numerical results were interesting as the low yield stress fluids converged correctly to the analytic solution (refer to Figures 3 and 4) especially at high flow rates, while the high yield stress fluids diverged with finer discretization (refer to Figures 5 and 6). This can be explained by the occurrence of plug flow at the middle of the tube which

is considerable in the case of high yield stress fluids. The minor deviation of the low yield stress fluids at low pressures highlights this fact since the plug flow effect diminishes as the pressure and flow rate increase. The failure of this approach for high yield stress fluids is simply because our model applies to fluids; and yield stress materials prior to yield at plug area behave like solids. The convergence of the low yield stress fluids is due to the fact that negligible plug occurs at the middle of the tube especially at high pressures.

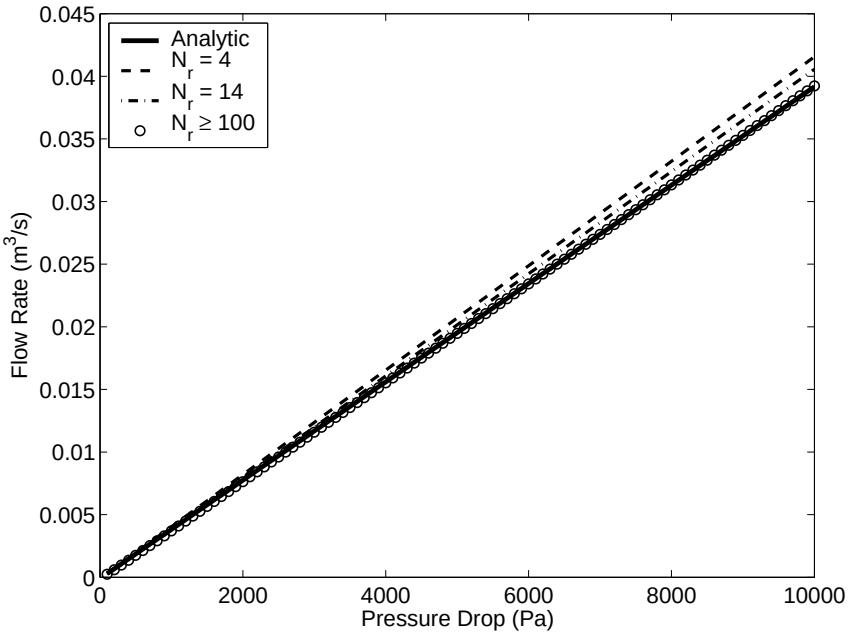

Figure 3: Q versus P plot for numeric solutions of a typical Bingham fluid above the yield point with $C = 0.01$ Pa.s and $\tau_o = 1.0$ Pa flowing in a tube with $L = 0.1$ m and $R = 0.01$ m for r-discretization $N_r = 4$, $N_r = 14$ and $N_r \geq 100$ alongside the analytic solution [1, 2].

5 Carreau and Cross Fluids

The Euler-Lagrange variational method was also applied to Carreau and Cross fluids for which no analytical expressions are available; the details are outlined in the following.

For Carreau fluids, the viscosity is given by [1, 11–14]

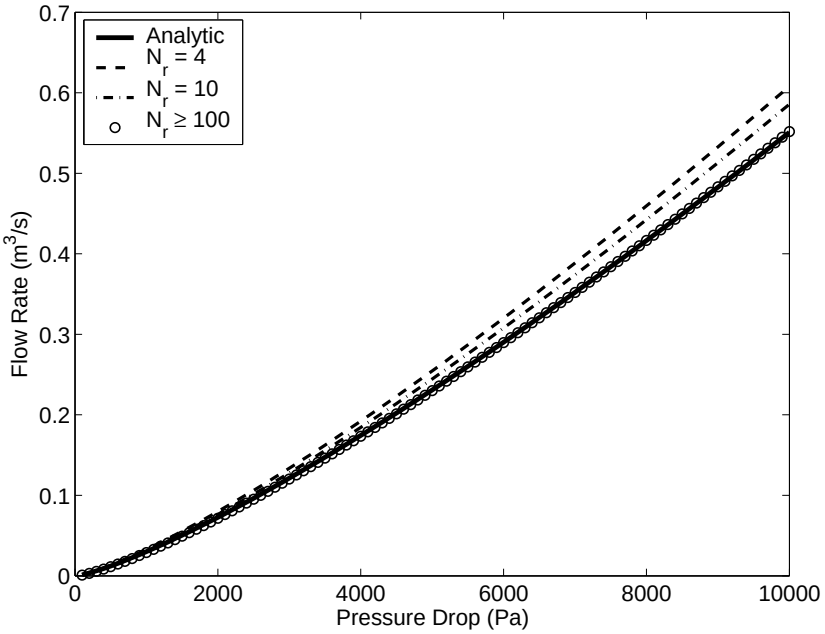

Figure 4: Q versus P plot for numeric solutions of a typical Herschel-Bulkley fluid above the yield point with $C = 0.01$ Pa.s^n, $n = 0.8$ and $\tau_o = 1.0$ Pa flowing in a tube with $L = 0.1$ m and $R = 0.01$ m for r-discretization $N_r = 4$, $N_r = 10$ and $N_r \geq 100$ alongside the analytic solution [1, 2].

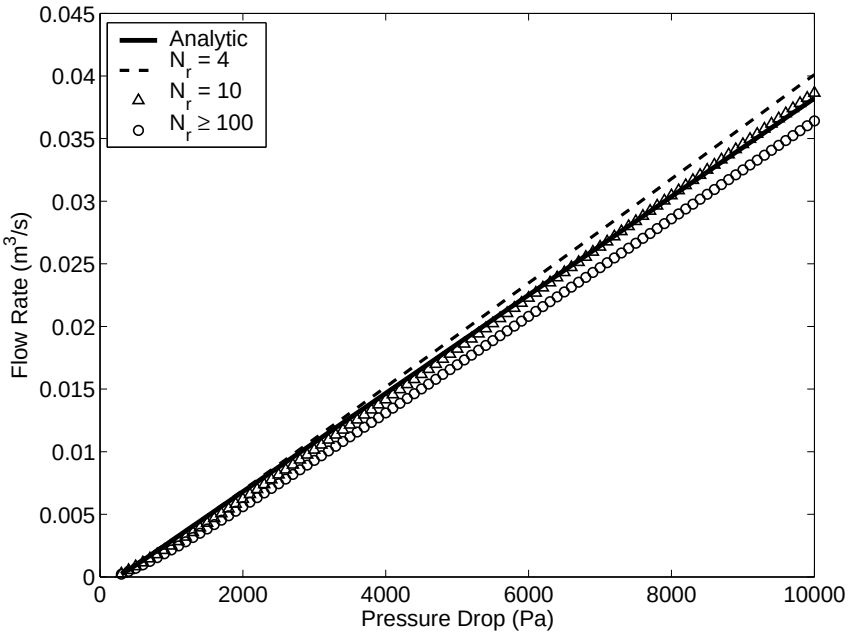

Figure 5: Q versus P plot for numeric solutions of a typical Bingham fluid above the yield point with $C = 0.01$ Pa.s and $\tau_o = 10.0$ Pa flowing in a tube with $L = 0.1$ m and $R = 0.01$ m for r-discretization $N_r = 4$, $N_r = 10$ and $N_r \geq 100$ alongside the analytic solution [1, 2].

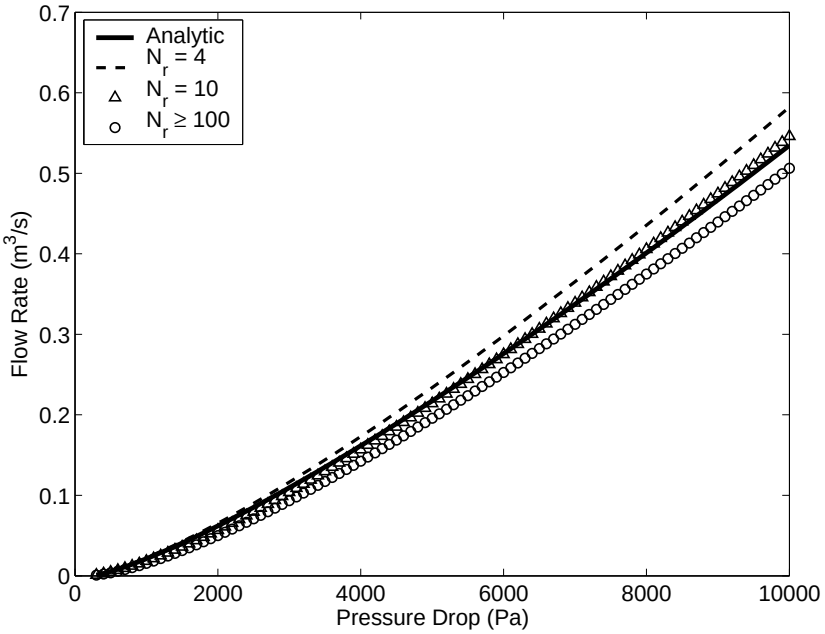

Figure 6: Q versus P plot for numeric solutions of a typical Herschel-Bulkley fluid above the yield point with $C = 0.01$ Pa.s^n, $n = 0.8$ and $\tau_o = 10.0$ Pa flowing in a tube with $L = 0.1$ m and $R = 0.01$ m for r-discretization $N_r = 4$, $N_r = 10$ and $N_r \geq 100$ alongside the analytic solution [1, 2].

$$\mu = \mu_\infty + (\mu_o - \mu_\infty)\left[1 + (\lambda\gamma)^2\right]^{(n-1)/2} \tag{38}$$

where μ_o is the zero-shear viscosity, μ_∞ is the infinite-shear viscosity, λ is a time constant, and n is the flow behavior index. On applying Euler-Lagrange variational principle (Equation 9) and following the derivation, as outlined in § 2.1 and 2.2, we obtain

$$\mu_\infty\gamma + (\mu_o - \mu_\infty)\,\gamma\,{}_2F_1\left(\frac{1}{2}, \frac{1-n}{2}; \frac{3}{2}; -\lambda^2\gamma^2\right) = Ar + B \tag{39}$$

where ${}_2F_1$ is the hypergeometric function, and A and B are the constants of integration. Now from the two boundary conditions at $r = 0$ and $r = R$, A and B can be determined, that is

$$\gamma\,(r = 0) = 0 \qquad \Rightarrow \qquad B = 0 \tag{40}$$

and

$$\gamma\left(r=R\right)=\gamma_w \qquad \Rightarrow \qquad \mu_\infty\gamma_w+\left(\mu_o-\mu_\infty\right)\gamma_w\,{}_2F_1\left(\frac{1}{2},\frac{1-n}{2};\frac{3}{2};-\lambda^2\gamma_w^2\right)=AR \tag{41}$$

where γ_w is the shear rate at the tube wall. Now, by definition we have

$$\tau_w=\mu_w\gamma_w \tag{42}$$

that is

$$\frac{PR}{2L}=\left[\mu_\infty+\left(\mu_o-\mu_\infty\right)\left[1+\left(\lambda\gamma_w\right)^2\right]^{(n-1)/2}\right]\gamma_w \tag{43}$$

From the last equation, γ_w can be obtained numerically by a numerical solver, based for example on a bisection method, and hence from Equation 41 A is obtained

$$A=\frac{\mu_\infty\gamma_w+\left(\mu_o-\mu_\infty\right)\gamma_w\,{}_2F_1\left(\frac{1}{2},\frac{1-n}{2};\frac{3}{2};-\lambda^2\gamma_w^2\right)}{R} \tag{44}$$

Several types of Carreau fluids were used for testing the model and its numerical implementation; a sample of these tests is presented in Figure 7 where the flow did converge for a radius discretization $N_r \geq 50$. A sample of the flow velocity profile across the tube for the fluid of Figure 7 at a typical flow condition is also presented in Figure 8. These figures are qualitatively correct despite the fact that no analytical solution is available to fully validate the results.

For Cross fluids, the viscosity is given by [15]

$$\mu=\mu_\infty+\frac{\mu_o-\mu_\infty}{1+\left(\lambda\gamma\right)^m} \tag{45}$$

where μ_o is the zero-shear viscosity, μ_∞ is the infinite-shear viscosity, λ is a time constant, and m is an indicial parameter. Following a similar derivation method

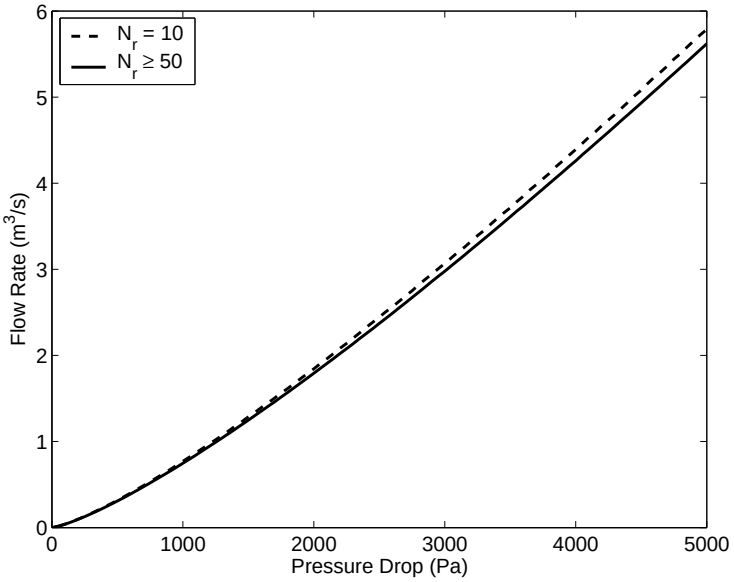

Figure 7: Q versus P plot for numeric solutions of a typical Carreau fluid with $n = 0.75$, $\mu_o = 0.05$ Pa.s, $\mu_\infty = 0.001$ Pa.s, and $\lambda = 1.0$ s flowing in a tube with $L = 0.5$ m and $R = 0.05$ m for r-discretization $N_r = 10$ and $N_r \geq 50$. The numeric solutions were obtained using the real part of the hypergeometric function ${}_2F_1$ in Equations 39 and 44.

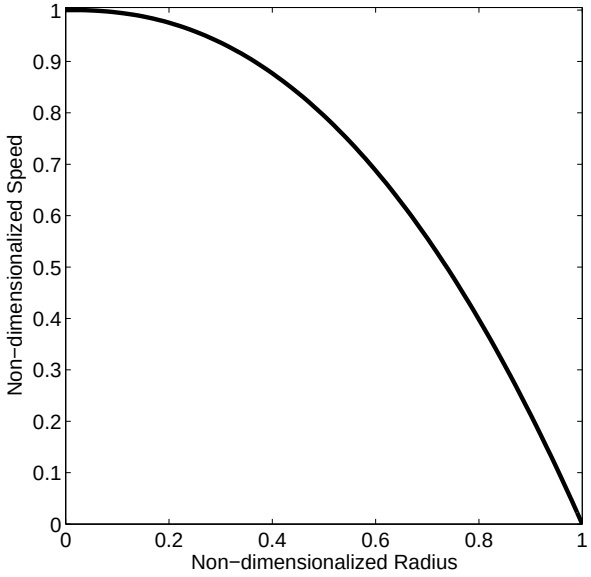

Figure 8: Flow velocity profile for the Carreau fluid of Figure 7 at a typical flow condition where the radius is scaled to unity and the speed is scaled to its maximum value at the tube center.

to that outlined in Carreau, we obtain

$$\mu_\infty \gamma + (\mu_o - \mu_\infty)\, \gamma\, {}_2F_1\left(1, \frac{1}{m}; \frac{m+1}{m}; -\lambda^m \gamma^m\right) = Ar \tag{46}$$

where

$$A = \frac{\mu_\infty \gamma_w + (\mu_o - \mu_\infty)\, \gamma_w\, {}_2F_1\left(1, \frac{1}{m}; \frac{m+1}{m}; -\lambda^m \gamma_w^m\right)}{R} \tag{47}$$

with γ_w being obtained numerically as outlined in Carreau.

Several types of Cross fluids were used for testing the model and its numerical implementation; a sample of these tests is presented in Figure 9 where the flow did converge for a radius discretization $N_r \geq 50$. A sample of the flow velocity profile across the tube for the fluid of Figure 9 at a typical flow condition is also presented in Figure 10. These figures are qualitatively correct despite the fact that no analytical solution is available to fully validate the results. The features in these results are similar to those observed in Carreau due to the strong similarities between these two fluids.

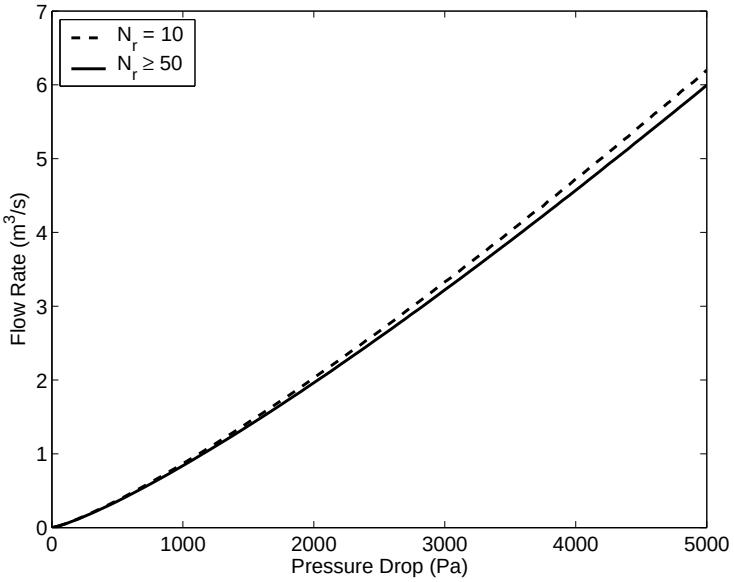

Figure 9: Q versus P plot for numeric solutions of a typical Cross fluid with $n = 0.25$, $\mu_o = 0.05$ Pa.s, $\mu_\infty = 0.001$ Pa.s, and $\lambda = 1.0$ s flowing in a tube with $L = 0.5$ m and $R = 0.05$ m for r-discretization $N_r = 10$ and $N_r \geq 50$. The numeric solutions were obtained using the real part of the hypergeometric function ${}_2F_1$ in Equations 46 and 47.

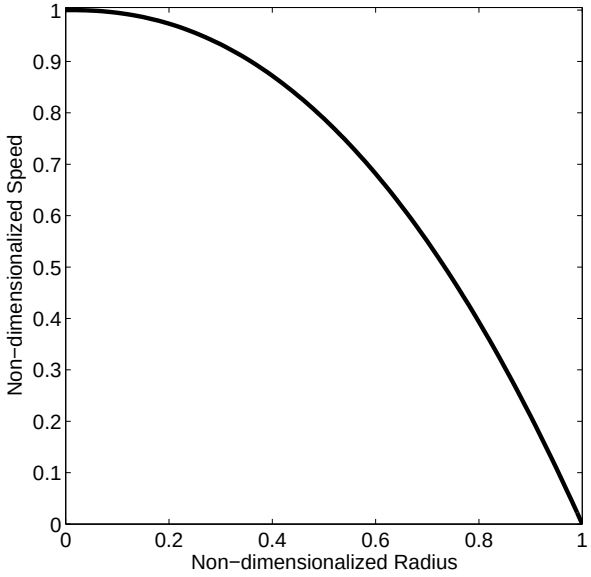

Figure 10: Flow velocity profile for the Cross fluid of Figure 9 at a typical flow condition where the radius is scaled to unity and the speed is scaled to its maximum value at the tube center.

6 Conclusions

In this article we outlined a method based on Euler-Lagrange variational principle which minimizes the total stress to obtain analytical and numerical flow relations for generalized Newtonian fluids in tubes and conduits in general. The method can be used in conjunction with numerical integration to obtain numerical solutions when analytical integration of the basic equations derived from the variational principle is difficult or impossible to obtain. The method was validated analytically and numerically for Newtonian fluids as well as a number of time-independent non-Newtonian fluids.

The main advantages of this method are simplicity, ease of implementation and rapid convergence to a solution which, for all practical purposes, is identical to the analytical solution. This convergence can be easily verified from two or more successive r-discretization schemes being converged to the same solution.

The method can be used to obtain flow relations for complex fluids for which no analytical flow expressions have been derived from other methods due to mathematical difficulties, such as Carreau, Carreau-Yasuda and Cross. This method, when implemented numerically in the case of analytical difficulties, is more accurate and suitable than the use of empirical relations or numerical meshing techniques.

Numerical experiments were performed on Bingham and Herschel-Bulkley yield stress fluids to test the robustness of this method which is based on the assumption of fluidity. Interestingly, the method converged correctly to the analytical solution for low yield stress fluids although it did diverge for high yield stress fluids. The obvious reason which can explain these observations is that negligible plug flow occurs at the middle of the tube in the first case especially at high flow rates, while considerable plug flow occurs in the second case which invalidates the basic assumption of fluidity that this model relies upon.

A preliminary investigation of the applicability of this method to Carreau and

Cross fluids has been conducted and presented in this article. More serious investigations related to these fluids and other complex fluids by employing this variational technique are planned for the future.

Nomenclature

γ	shear rate (s^{-1})
γ_w	shear rate at tube wall (s^{-1})
λ	time constant (s)
μ	fluid dynamic shear viscosity (Pa.s)
μ_o	zero-shear viscosity (Pa.s)
μ_∞	infinite-shear viscosity (Pa.s)
τ	shear stress (Pa)
τ_c	shear stress at tube center (Pa)
τ_o	yield stress (Pa)
τ_t	total shear stress (Pa)
τ_w	shear stress at tube wall (Pa)
C	consistency factor in Bingham and Herschel-Bulkley models ($Pa.s^n$)
${}_2F_1$	hypergeometric function
k	consistency factor in power law model ($Pa.s^n$)
L	tube length (m)
m	indicial parameter in Cross model
n	flow behavior index
N_r	number of elements in radius discretization
p	pressure (Pa)
P	pressure drop (Pa)
Q	volumetric flow rate ($m^3.s^{-1}$)
r	radius (m)

R tube radius (m)

v axial fluid velocity ($\mathrm{m.s^{-1}}$)

References

[1] T. Sochi. *Pore-Scale Modeling of Non-Newtonian Flow in Porous Media*. PhD thesis, Imperial College London, 2007. 3, 6, 11, 14, 15, 16, 17, 18

[2] T. Sochi; M.J. Blunt. Pore-scale network modeling of Ellis and Herschel-Bulkley fluids. *Journal of Petroleum Science and Engineering*, 60(2):105–124, 2008. 3, 6, 11, 14, 15, 16, 17, 18

[3] A.H.P. Skelland. *Non-Newtonian Flow and Heat Transfer*. John Wiley and Sons Inc., 1967. 6, 11

[4] T. Sochi. Newtonian Flow in Converging-Diverging Capillaries. Submitted. 6

[5] T. Sochi. The flow of power-law fluids in axisymmetric corrugated tubes. *Journal of Petroleum Science and Engineering*, 78(3-4):582–585, 2011. 6, 11

[6] P.J. Carreau; D. De Kee; R.P. Chhabra. *Rheology of Polymeric Systems*. Hanser Publishers, 1997. 6

[7] T. Sochi. Pore-scale modeling of viscoelastic flow in porous media using a Bautista-Manero fluid. *International Journal of Heat and Fluid Flow*, 30(6):1202–1217, 2009. 6

[8] T. Sochi. Slip at Fluid-Solid Interface. *Polymer Reviews*, 51:1–33, 2011. 6

[9] T. Sochi. Computational Techniques for Modeling Non-Newtonian Flow in Porous Media. *International Journal of Modeling, Simulation, and Scientific Computing*, 1(2):239–256, 2010. 14, 15

[10] T. Sochi. Modelling the Flow of Yield-Stress Fluids in Porous Media. *Transport in Porous Media*, 85(2):489–503, 2010. 14, 15

[11] K.S. Sorbie. *Polymer-Improved Oil Recovery*. Blakie and Son Ltd, 1991. 16

[12] T. Sochi. Flow of Non-Newtonian Fluids in Porous Media. *Journal of Polymer Science Part B*, 48(23):2437–2467, 2010. 16

[13] T. Sochi. Non-Newtonian Flow in Porous Media. *Polymer*, 51(22):5007–5023, 2010. 16

[14] R.I. Tanner. *Engineering Rheology*. Oxford University Press, 2nd edition, 2000. 16

[15] R.G. Owens; T.N. Phillips. *Computational Rheology*. Imperial College Press, 2002. 19